Neuron
Article

Gamma Oscillations Are Generated Locally in an Attention-Related Midbrain Network

C. Alex Goddard,[1,3,*] Devarajan Sridharan,[1,3,*] John R. Huguenard,[2] and Eric I. Knudsen[1]
[1]Department of Neurobiology
[2]Department of Neurology
Stanford University, Stanford, CA 94305, USA
[3]These authors contributed equally to this work
*Correspondence: cgoddard@stanford.edu (C.A.G.), dsridhar@stanford.edu (D.S.)
DOI 10.1016/j.neuron.2011.11.028

SUMMARY

Gamma-band (25–140 Hz) oscillations are a hallmark of sensory processing in the forebrain. The optic tectum (OT), a midbrain structure implicated in sensorimotor processing and attention, also exhibits gamma oscillations. However, the origin and mechanisms of these oscillations remain unknown. We discovered that in acute slices of the avian OT, persistent (>100 ms) epochs of large amplitude gamma oscillations can be evoked that closely resemble those recorded in vivo. We found that cholinergic, glutamatergic, and GABAergic mechanisms differentially regulate the structure of the oscillations at various timescales. These persistent oscillations originate in the multisensory layers of the OT and are broadcast to visual layers via the cholinergic nucleus Ipc, providing a potential mechanism for enhancing the processing of visual information within the OT. The finding that the midbrain contains an intrinsic gamma-generating circuit suggests that the OT could use its own oscillatory code to route signals to forebrain networks.

INTRODUCTION

Gamma (25–140 Hz) oscillations of the local field potential (LFP) in the forebrain reflect a synchronization of synaptic inputs that may be crucial for preferential processing of sensory information and for attention (Fries, 2009). Recent research demonstrates that a midbrain structure, the optic tectum (OT, called the superior colliculus, SC, in mammals), also exhibits large amplitude, spatially localized gamma oscillations in response to sensory stimulation in vivo (Sridharan et al., 2011). The OT/SC is a critical node in a midbrain network that interacts extensively with the forebrain to control the direction of gaze and the locus of attention (Knudsen, 2011).

What is the source of the gamma oscillations in the midbrain network? The oscillations could result from descending, rhythmic input from the forebrain (Fries, 2009). Alternatively, the midbrain might be capable of generating its own oscillations. A midbrain source of gamma oscillations with mechanisms similar to those in forebrain networks would suggest that the circuits for generating such oscillations, as well as their role in information processing, are conserved across embryologically distinct brain structures. Furthermore, as gamma oscillations are posited to provide a channel for communication between cortical areas during sensory processing and attention (Gregoriou et al., 2009), a midbrain source of gamma oscillations would allow the OT to deliver signals of spatial priority (Fecteau and Munoz, 2006) to the forebrain using synchronized spikes. This study investigates the source and mechanisms of gamma oscillations in the midbrain.

Gamma oscillations have been investigated extensively in the mammalian forebrain. They are evoked in sensory cortical areas by salient stimuli of various modalities, and gamma oscillation power is modulated in prefrontal, parietal, and sensory cortical areas by attention (Engel et al., 2001). A hallmark of these oscillations is a rhythmic interplay of excitatory and inhibitory currents (Bartos et al., 2007). Cholinergic and glutamatergic agonists facilitate oscillations by enhancing the excitability of the oscillation-generating circuitry (Fisahn et al., 1998; Roopun et al., 2010). Ionotropic GABA receptors (GABA-R) regulate the periodicity of the oscillations and can gate the timing of neuronal discharges, creating synchronized activity at the population level for enhanced intracortical communication (Bartos et al., 2007).

Neural activity with gamma periodicity has also been observed in the OT/SC (Brecht et al., 1999; Neuenschwander et al., 1996; Sridharan et al., 2011). The OT/SC is a multilayered structure that is part of a midbrain network that plays an essential role in gaze and attention (Knudsen, 2011). The OT/SC itself contains two major components of the midbrain network, both organized in a topographic map of space. One component, the superficial layers (sOT; layers 1–9 in avians; Figure 1A, bar), represents the locations of salient visual stimuli. Another component, the intermediate and deep layers (i/dOT; layers 10–15 in avians), represents the locations of salient stimuli for multiple sensory modalities as well as the goals of orienting movements.

The flow of information through the midbrain network has been reviewed recently (Knudsen, 2011). Visual information propagates directly from the retina to the sOT. This information reaches the i/dOT via projections from the sOT as well as by direct retinal input onto i/dOT dendrites (Figure 1B). The i/dOT also receives multisensory spatial information and movement-related signals from the brainstem and forebrain. A special class of

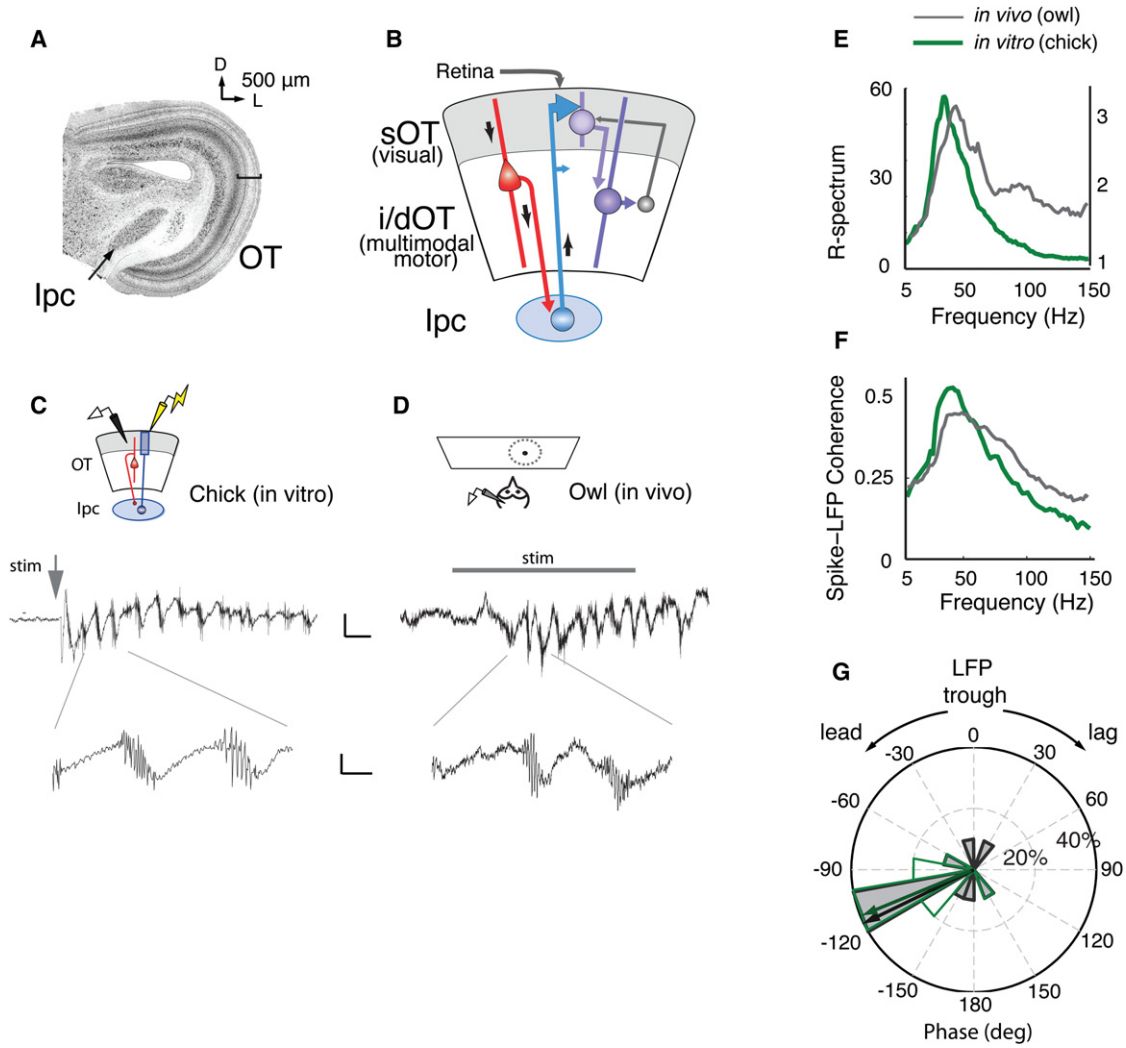

Figure 1. In Vivo-like Oscillations in an In Vitro Slice of the Avian Midbrain

(A) Left, low-power image of a transverse, Nissl-stained section of the chicken midbrain. The nucleus isthmi pars parvocellularis (Ipc) is located medial to the optic tectum (OT). Bar indicates the sOT. D: Dorsal, L: Lateral.

(B) Schematic of the chick midbrain circuitry. Retinal afferents enter from the most superficial aspect of the sOT, contacting both sOT and i/dOT neurons. A subclass of i/dOT neurons in layer 10 (red) project to the Ipc (blue), which in turn sends projections heavily to the sOT and to a lesser degree to the i/dOT. Feedback projections from the i/dOT to the sOT also exist (gray).

(C) Top, schematic of the in vitro slice preparation of the chick midbrain. An extracellular recording electrode (black) and a stimulating electrode (yellow) were placed in the sOT. Middle, in vitro oscillations in the superficial layers of a chicken midbrain slice in response to a single, 10 μA, 0.1 ms electrical stimulus (gray arrow) delivered to the retinal afferents. Scale bar: 50 ms, 20 μV. Bottom, expanded time scale showing a high-frequency burst of spikes riding on top of the lower frequency (gamma-band) field potential. Scale bar: 10 ms, 10 μV.

(D) Top, schematic of the in vivo preparation in the owl OT. An extracellular recording electrode was lowered into the sOT, and a small, moving dot was presented in the receptive field of the site. Middle, in vivo oscillations in the sOT of the owl optic tectum in response to 350 ms visual stimulation (gray bar). Scale bar: 50 ms, 10 μV. Bottom, expanded time scale showing a high-frequency burst of spikes riding on top of the lower frequency (gamma-band) field potential. Scale bar: 10 ms, 5 μV.

(E) Average ratio spectra (R-spectra) of the oscillations recorded from chicken sOT in vitro (green, thick line, n = 10 slices) and owl sOT in vivo (gray, thin line, n = 10 sites) showing a dominant peak in relative power in the low-gamma band (25–50 Hz). y axis on left for in vitro recordings; y axis on right for in vivo.

(F) Spike field coherence (SFC) measured in the sOT from in vitro (green, thick line) and in vivo (gray, thin line) preparations (same recordings as in [E]). The SFC in both preparations shows a clear peak in the low-gamma band.

(G) Phase relationship of the spikes relative to the trough of the LFP in the 25–50 Hz frequency range from in vitro (green line, no fill) and in vivo (black line, gray fill) preparations (same recordings as in [E and F]). Spikes precede the LFP trough by ~120° of gamma phase. Radial axis: percent of sites. Arrows: median phase.

neurons, located in layer 10 (Figure 1B, red), receives input from both the sOT and the i/dOT and projects to the various nuclei in the isthmic complex: specialized cholinergic, GABAergic, and glutamatergic circuits that support global competition and stimulus selection (Mysore et al., 2010; Asadollahi et al., 2010; Gruberg et al., 2006). The isthmic nuclei send information back

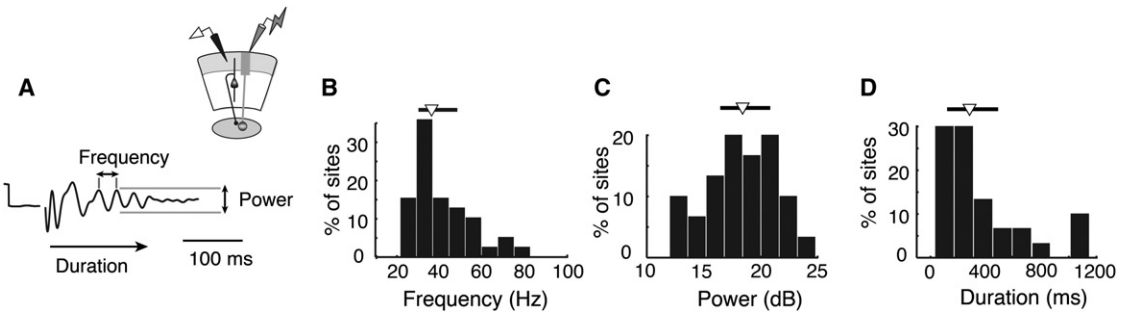

Figure 2. Summary of Gamma Oscillation Properties in the sOT Recorded In Vitro

All data represent distributions across 39 sites. For B-D, median and 95% confidence interval (ci) are denoted above the histogram by an inverted triangle and solid line, respectively.

(A) Top, schematic illustrating recording configuration in the sOT. Bottom, diagram of an evoked oscillation bandpass filtered between 5–200 Hz, and the three metrics computed for LFP oscillations: gamma frequency, power, and duration.

(B) Distribution of peak frequencies of gamma periodicity. Median frequency = 36.1 Hz and 95% ci = 29.5–46.9 Hz.

(C) Distribution of power of gamma (25–50 Hz) oscillations. Median power = 18.42 dB and 95% ci = 16.45–20.85 dB.

(D) Distribution of gamma oscillation durations. Median duration = 284 ms and 95% ci = 140–477 ms.

to both the sOT and i/dOT. Outputs from the sOT project to vision-related structures in the brainstem and thalamus, and outputs from the i/dOT project to various nuclei in the thalamus and to movement-generating circuitry in the brainstem and spinal cord.

One of the isthmic nuclei, the nucleus isthmi pars parvocellularis (Ipc; called the parabigeminal nucleus in mammals, Graybiel, 1978), is of particular relevance with regard to midbrain gamma oscillations. The Ipc is a cholinergic nucleus that interconnects reciprocally and topographically with the OT (Figure 1B, blue; Wang et al., 2006). Ipc neurons respond to visual and auditory stimuli and send synchronized bursts with gamma periodicity back to the sOT (Asadollahi et al., 2010). Because of this latter property, the Ipc could be the source of the gamma oscillations that are observed in the OT. This possibility is reinforced by the observation that cholinergic input can induce gamma oscillations in the mammalian neocortex and hippocampus (Fisahn et al., 1998; Rodriguez et al., 2004).

Here, we report that gamma oscillations, closely resembling those recorded in vivo, can be evoked in a slice preparation of the midbrain network. We explore the synaptic mechanisms that regulate the structure of these oscillations at various timescales and show that the mechanisms are remarkably similar to those that regulate the structure of forebrain gamma oscillations. By systematic anatomical, physiological, and pharmacological deconstruction of the midbrain network, we show that the circuitry that generates the gamma oscillations resides in the multisensory i/dOT. These oscillations are then broadcast to the sOT via the Ipc to create spatially constrained columns of coordinated gamma rhythmicity across the input and output layers of the OT.

RESULTS

Gamma Oscillations Are Intrinsic to the Midbrain

To test whether gamma oscillations are generated locally within the midbrain, we developed an acute slice preparation of the chicken midbrain. Thick (400 micron) sections were cut in a transverse plane that preserved the reciprocal, homotopic connections between the OT and the Ipc (Figures 1A and 1B). In response to electrical stimulation of retinal afferents, high-amplitude gamma oscillations were recorded in vitro in the superficial layer 5 of the sOT (Figure 1C), with a median frequency of 36 Hz (95% conf. interval = 29.5–46.9 Hz, Figures 1E and 2B). The LFP oscillations observed in vitro bore striking resemblance to those evoked by visual stimuli in the barn owl OT in vivo (Figures 1D and 1E). Both in vitro and in vivo, oscillations in the sOT exhibited peak spectral power (ratio of induced to baseline power, or R-spectrum) in the 25–50 Hz frequency range and were precisely phase-locked to spike bursts in this range (Figures 1, 1F, 1G, S1A, available online, and S1B). The remarkable similarity of the microstructure of the oscillations in vitro and in vivo demonstrates that the midbrain itself contains a network that generates gamma oscillations in response to afferent input.

Oscillations evoked in vitro were persistent: a single 0.1 ms electrical pulse, delivered to the retinal afferents, evoked oscillations in the sOT that typically lasted more than 150 ms (Figure 2D). In contrast to many forebrain slice preparations, these in vitro oscillations did not require the addition of neurotransmitter receptor agonists to the bath. Moreover, oscillations could be evoked in solutions with relatively low K^+ and high Mg^{2+}, which bias the network toward lower excitability, or in solutions with relatively high K^+ and low Mg^{2+}, which bias the network toward higher excitability (Figures S1C, S1D, S1E, and S1F). Thus, the activation of this oscillator was robust to ionic manipulation of network excitability.

Midbrain Gamma Oscillations Are Regulated by GABA, NMDA, and ACh Receptors

We next examined whether pharmacological mechanisms that control gamma oscillations in forebrain areas also control midbrain oscillations. We tested the effects of bath-applied receptor blockers on the frequency, amplitude, and duration of LFP oscillations in the sOT in vitro (Figure 2A). To capture properties of the persistent oscillations, and not of the transients

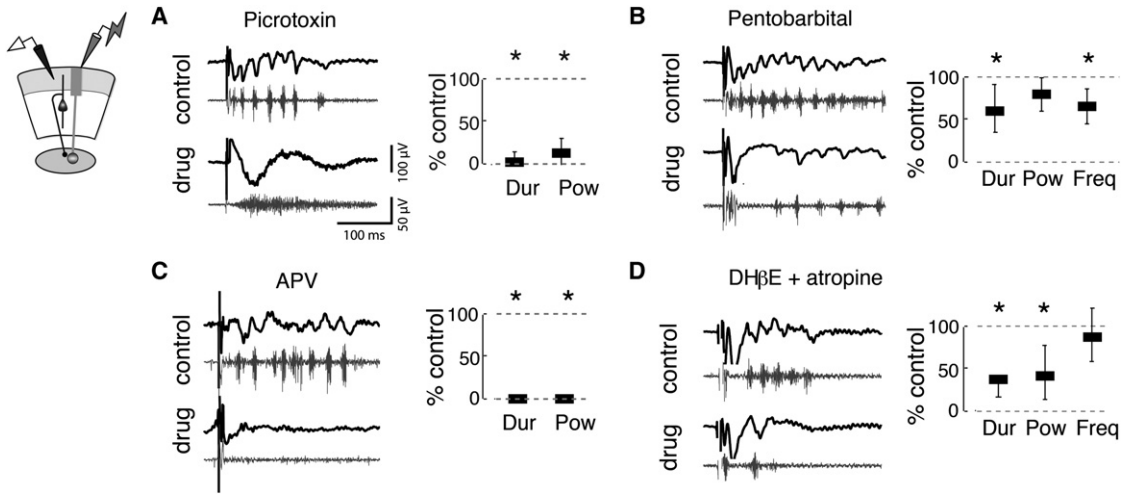

Figure 3. Multiple Neurotransmitter Systems Contribute to Gamma Oscillations in the OT

Left panels, black traces show representative traces bandpass filtered between 5–200 Hz. Gray traces show the traces highpass filtered above 250 Hz. Right panels, power, frequency, and duration were computed using LFPs filtered from 25–50 Hz. Bars represent medians and whiskers represent 25th and 75th percentiles; bar thickness has no meaning. All drugs were applied to the bath. All p-values calculated with Friedman tests and are Bonferroni corrected for multiple comparisons.

(A) Far left, schematic illustrating recording configuration in sOT. Right middle, picrotoxin (PTX, 10 μM) converted gamma oscillations to episodes of high-frequency spiking. Duration (2.9% of control) in the gamma band and gamma power (13.7% of control) of oscillations were significantly reduced ($p < 0.001$, $n = 6$ slices).

(B) $GABA_A$–R enhancer pentobarbital (10 μM) significantly reduced the duration (60.2% of control) and frequency (69.8% of control) of oscillations ($p < 0.001$, $n = 6$), but did not alter gamma power ($p = 0.14$).

(C) NMDA-R antagonist APV (20 μM) abolished gamma oscillations. Both duration and power of gamma oscillations were eliminated (both are 0% of control, $p < 0.001$, $n = 4$).

(D) ACh-R antagonists DHβE (40 μM) and atropine (5 μM) significantly reduced the duration (44.4% of control) and gamma power (61.2% of control) of oscillations ($p < 0.001$, $n = 6$). Frequency (87.9% of control) of gamma oscillations was unaffected ($p > 0.9$).

associated with the stimulus artifact, we excluded the initial 50 ms of signal post-stimulus from analysis and subtracted the stimulus-locked component of the signal. In keeping with previous nomenclature, we refer to these as induced oscillations (Gandal et al., 2011).

First, we tested the contribution of GABA-R to the oscillations. In the mammalian neocortex and hippocampus, inhibitory $GABA_A$-Rs regulate the frequency of gamma oscillations (Bartos et al., 2007). We first blocked $GABA_{A,C}$-Rs (and glycine-Rs) with bath-applied picrotoxin (PTX, 10 μM). PTX converted episodes of gamma periodicity into episodes of high-frequency spiking activity in the sOT (Figures 3A, S2A, and S2B). Both the power and duration of oscillations in the gamma-band were strongly diminished: power was 14% of control and duration was 3% of control ($p < 0.001$, Friedman test, $n = 6$; Figure 3A). This result suggested that GABA-R activity was critical for generating activity with gamma periodicity. We then tested whether the kinetics of GABA-Rs pace the oscillations by applying pentobarbital. Pentobarbital prolongs the duration of $GABA_A$ currents by increasing the duration of channel openings following the binding of GABA to the receptor. Pentobarbital shortened the duration (60% of control; $p < 0.001$, $n = 6$) and slowed the frequency (70% of control, $p < 0.001$, $n = 6$) but did not alter the power of the oscillations (Figures 3B and S2C). Thus, GABA-Rs were necessary for gamma periodicity and they regulated oscillation frequency.

Next, we tested the contribution of NMDA-Rs to the oscillations. A conspicuous feature of the OT oscillations was their persistence for up to hundreds of milliseconds following induction (Figure 2D). The persistence of nonoscillatory, spiking activity observed in the rodent and frog OT is known to depend on NMDA-Rs (Isa and Hall, 2009; Pratt et al., 2008). We found that bath application of the NMDA-R antagonist APV (50 μM) dramatically shortened induced gamma oscillations (Figures 3C, S2D, and S2E) such that they never exceeded 50 ms; no gamma power above baseline was observed during the poststimulus window ($p < 0.001$, Friedman test, $n = 4$). Thus, NMDA-R activity was necessary for the persistence of gamma oscillations in the sOT.

Finally, we tested the contribution of acetylcholine receptors (ACh-Rs) to the oscillations. ACh-Rs have been implicated in the generation and modulation of gamma oscillations in the mammalian forebrain (Fisahn et al., 1998; Rodriguez et al., 2004). In the avian midbrain network, neurons in the OT and Ipc exhibit strong immunoreactivity for the synthetic enzyme for ACh (Wang et al., 2006) and, in the fish midbrain, activation of the isthmic nuclei enhances OT responses to retinal afferent stimulation in an ACh-R-dependent manner (King and Schmidt, 1991). We found that concurrent addition of both muscarinic and nicotinic ACh-R blockers, atropine (5 μM) and DHβE (40 μM), to the bath reduced the duration of oscillations to 44% of control, and power to 61% of control ($p < 0.001$,

Friedman test, n = 5), but did not alter oscillation frequency (88% of control, $p > 0.9$, n = 5, Figures 3D and S2F). Thus, ACh-Rs modulated the excitability of the oscillator but were not required for generating or pacing oscillations in the sOT.

Ipc Neurons Intrinsically Burst at Gamma Frequencies but Do Not Generate Persistent Oscillations

Having identified pharmacological mechanisms that regulate oscillation structure, we sought to locate the source of the midbrain oscillations. Gamma oscillations in the sOT included bursts of spikes that were phase-locked to each cycle of the LFP (Figures 1F and 1G). These spikes are not discharges of sOT neurons, but rather of Ipc axons (Marín et al., 2005), which have exceptionally large diameters and form dense fields of terminals, particularly in layers 2–6 of the OT (Figure S3A). Because Ipc neurons burst with gamma periodicity in vivo (Asadollahi et al., 2010), the Ipc is a likely candidate source of gamma oscillations in the sOT. We discovered a consistent relationship between the strength of sOT spike bursts and the amplitude of the LFP (Figures S3B, S3C, S3D, and S3E). Specifically, the amount of spike activity in a burst correlated with the amplitude of the LFP that followed the burst (mean correlation: $r = 0.48$, greater than zero, $p < 0.05$, Wilcoxon signed-rank test, n = 10 sites, Figures S3C, S3D, and S3E). This correlation was not significant for the preceding LFP ($r = 0.20$, not different from zero, $p > 0.05$, Wilcoxon signed-rank test), indicating that the observed correlation was not due to trial-by-trial variation in overall signal amplitude. This result demonstrates that the sOT LFP reflects, on a cycle-by-cycle basis, the strength of the periodic input from the Ipc.

We then tested the necessity of the Ipc for generating persistent gamma oscillations in the sOT by comparing two types of slices: slices with intact connections between the OT and the Ipc (intact slices) and slices with these connections surgically transected (transected slices, Figure S4A). Transection eliminated induced gamma oscillations in the sOT (gamma power: intact = 16 dB, transected = 0 dB, $p < 0.01$; duration: intact: 332 ms, transected = 0 ms, $p < 0.01$, Mann-Whitney U-test, n = 10, Figures 4A, 4B, and 4C). Similarly, focal blockade of AMPAergic synaptic excitation in the Ipc with microinjections of CNQX also eliminated oscillations in the sOT (Figures 4D and 4E). These results confirmed that the gamma oscillations recorded in the sOT result from Ipc input.

Although the Ipc is required for the expression of gamma oscillations in the sOT, is the Ipc a gamma generator itself? We tested whether Ipc neurons are capable of generating oscillatory activity intrinsically by recording from them intracellularly. Upon sustained depolarization, Ipc neurons fired rhythmic bursts of spikes at low gamma frequencies that increased systematically from 14 to 56 Hz with increasing membrane depolarization (Figures 5A and 5B). Thus, Ipc neurons are intrinsically tuned to burst with low gamma periodicity when depolarized.

The question remained, however, as to whether the Ipc can generate persistent gamma oscillations in response to transient activation, as observed in the sOT of intact slices. To address this question, we activated the isolated Ipc directly with electrical microstimulation in transected slices. This manipulation induced brief bursts of Ipc spikes but did not cause the neurons to fire persistently (Figures S4B and S4D, median duration of response = 5 ms), suggesting that transient activation of the Ipc alone is inadequate to generate persistent oscillations.

This suggestion was reinforced by results from a different experimental manipulation. Spontaneous gamma oscillations were observed in the Ipc in intact slices when they were bathed in a high-excitability solution (high K^+, low Mg^{2+}; see Experimental Procedures). We tested whether these spontaneous oscillations would persist in transected slices (Figures 5C, S4C, S4D, and S4E). In intact slices, 15 ± 9% of the spontaneous Ipc oscillations had durations ≥ 150 ms (n = 6), whereas in transected slices, persistent Ipc oscillations were exceedingly rare (0.2 ± 0.4%, $p < 0.005$, n = 5). Therefore, Ipc neurons, though tuned to burst at low gamma frequencies, did not generate persistent oscillations when isolated from the OT.

These results implied that the persistent, spontaneous oscillations observed in the Ipc of intact slices depend on extrinsic, persistent drive. To test this inference, we recorded intracellularly from Ipc neurons in intact slices during epochs of gamma oscillations. Under these conditions, Ipc neurons at resting potential discharged in bursts of spikes in the gamma band (Figures 5D and 5E). When hyperpolarized, these neurons exhibited barrages of subthreshold excitatory postsynaptic potentials with gamma periodicities that closely matched the periodicity of spiking discharges (Figures 5D and 5E). Because the only remaining source of input to the Ipc in these slices was the layer 10 neurons in the multisensory i/dOT (Wang et al., 2006), these results indicate that Ipc neurons burst persistently and periodically in response to rhythmic input from the OT.

Midbrain Gamma Oscillations Are Generated in the Multisensory i/dOT

The observations that Ipc neurons 1) are entrained by periodic input and 2) do not generate persistent oscillations when isolated from the OT suggest that either the Ipc is part of the gamma generating mechanism itself or that it receives input from a gamma generator in the i/dOT. To distinguish between these possibilities, we investigated whether the OT is capable of generating gamma oscillations on its own.

In intact slices, retinal afferent stimulation evoked persistent oscillations not only in the sOT but also in the i/dOT (layers 10–15, Figures 6A, 6B, and 6C). The power spectrum of the oscillations was substantially broader in the i/dOT than in the sOT (Figures 6B, S5A, and S5B): oscillation power in the i/dOT was distributed across both low (25–90 Hz) and high (90–140 Hz) gamma frequencies. This result mirrored observations made in vivo, where the power spectrum of gamma oscillations induced by a visual stimulus was broader in the i/dOT than in the sOT (Figures S5C and S5D).

To test whether the OT alone can generate persistent gamma activity, we recorded multiunit spike and LFP activity in the i/dOT in transected slices. OT-Ipc transection, which simultaneously eliminated gamma activity in the sOT as described above (Figures S5E and S5F, top), did not eliminate gamma activity in the i/dOT (Figures S5E and S5F, bottom): retinal afferent stimulation continued to induce persistent, broadband gamma oscillations in the i/dOT (median power in intact slices = 13.2 dB, transected = 11.4 dB, $p > 0.2$, U-test, n = 10, Figures 6A, 6B,

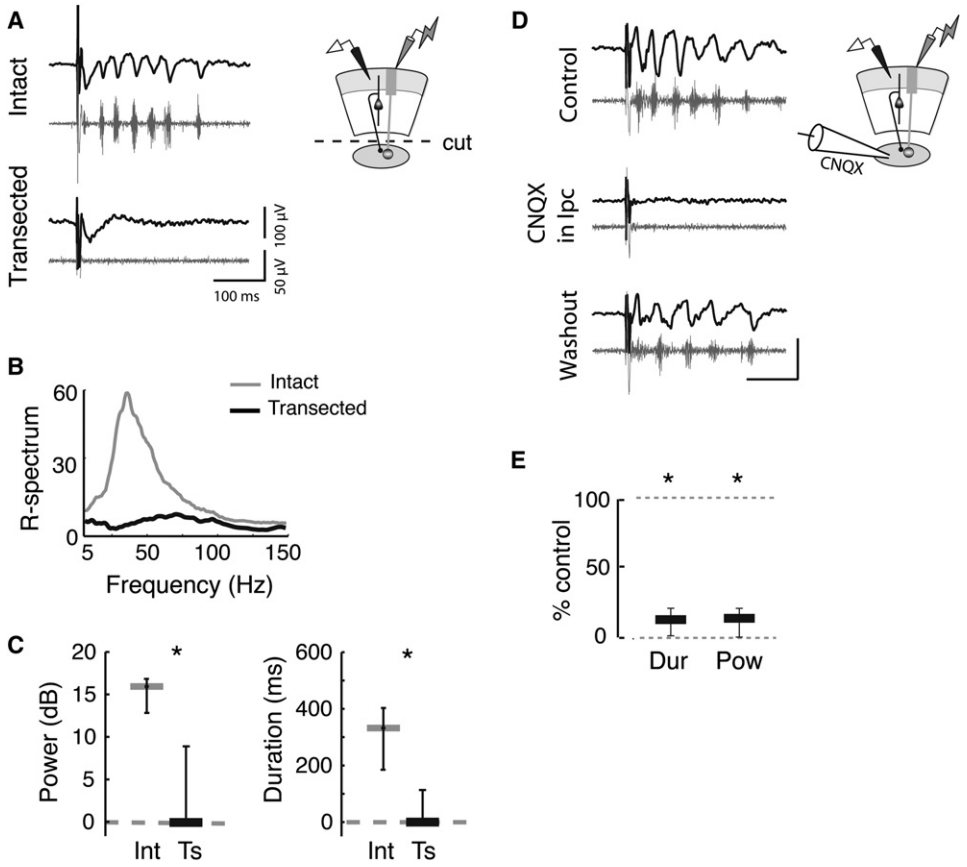

Figure 4. Ipc Is Required for Gamma Oscillations in the sOT

Conventions are as in Figure 3.

(A) Left, evoked gamma oscillations (top) were eliminated from the sOT when connections with the Ipc were transected (bottom). Right, schematic illustrating transection of Ipc connections and recording configuration in sOT.

(B) Power spectra of activity in the sOT in intact slices (gray) and in transected slices (black).

(C) Left, gamma power in sOT in intact slices (Int) is abolished in transected (Ts) slices (intact = 16 dB, transected = 0 dB, $p < 0.01$, U-test, n = 10). Right, persistence of gamma oscillations in sOT is eliminated in transected slices (intact = 332 ms, transected = 0 ms, $p < 0.01$).

(D) Left, oscillations recorded in the sOT of intact slices were reversibly eliminated following focal application of the glutamatergic blocker CNQX to the Ipc. 0.5 mM CNQX was puffed for 0.5–1 s at 5 psi from a patch pipette above the slice in the Ipc. Puffs were administered such that bath flow was moving away from the OT, to prevent synaptic blockade of OT circuitry. Right, schematic illustrating focal puffing of CNQX into the Ipc and recording configuration in the sOT.

(E) Both gamma duration and power in the sOT of intact slices were significantly reduced relative to control following application of CNQX to the Ipc (duration: 11.5% of control, $p < 0.001$; power: 13.5% of control, $p < 0.001$, Friedman test, n = 5,); both recovered in 60% (n = 3/5) of the sites.

and 6C). Furthermore, the oscillations were persistent, although a trend toward shortened durations was noted in transected slices (median: 172 ms, $p > 0.1$ compared to durations in intact slices, n = 10, Figure 6C).

A rhythmic interplay of excitatory and inhibitory currents is a hallmark of gamma-generating networks (Bartos et al., 2007). We made whole-cell patch clamp recordings from layer 10 neurons in the i/dOT to test whether postsynaptic currents (PSCs) were correlated with the LFP simultaneously recorded extracellularly < 100 μm away. Retinal afferent stimulation evoked persistent barrages of EPSCs and IPSCs that exhibited strong gamma coherence with the LFP, with peaks in the low-gamma band (25–50 Hz; Figures 6D, S5G, and S5H, n = 17 neuron-field pairs). Analysis of the phase of the cross-spectrum between the PSCs and the LFP revealed that EPSCs led IPSCs by 53 ± 14 degrees of gamma cycle phase (Figure 6E), a lead of 4.0 ± 1.0 ms (mean ± SEM, n = 17, $p < 0.01$, Wilcoxon signed-rank test). In addition, we constructed a 25–50 Hz LFP trough-triggered average of the intracellularly recorded EPSCs and IPSCs. This analysis revealed low-gamma periodicity in the average PSC waveforms (Figure 6F). In addition, the EPSCs peaked at the trough of the LFP and the IPSCs peaked shortly thereafter (Figure 6F and S5I). Moreover, extracellular recordings from single neurons in layer 10 of transected slices revealed that these neurons tended to fire persistently with gamma periodicity (median: 32.5 Hz; Figure S5J). Together, these data demonstrate that a circuit intrinsic to the OT can generate and maintain persistent gamma oscillations.

If the generator of these oscillations is indeed located in the OT, then the pharmacological manipulations that altered

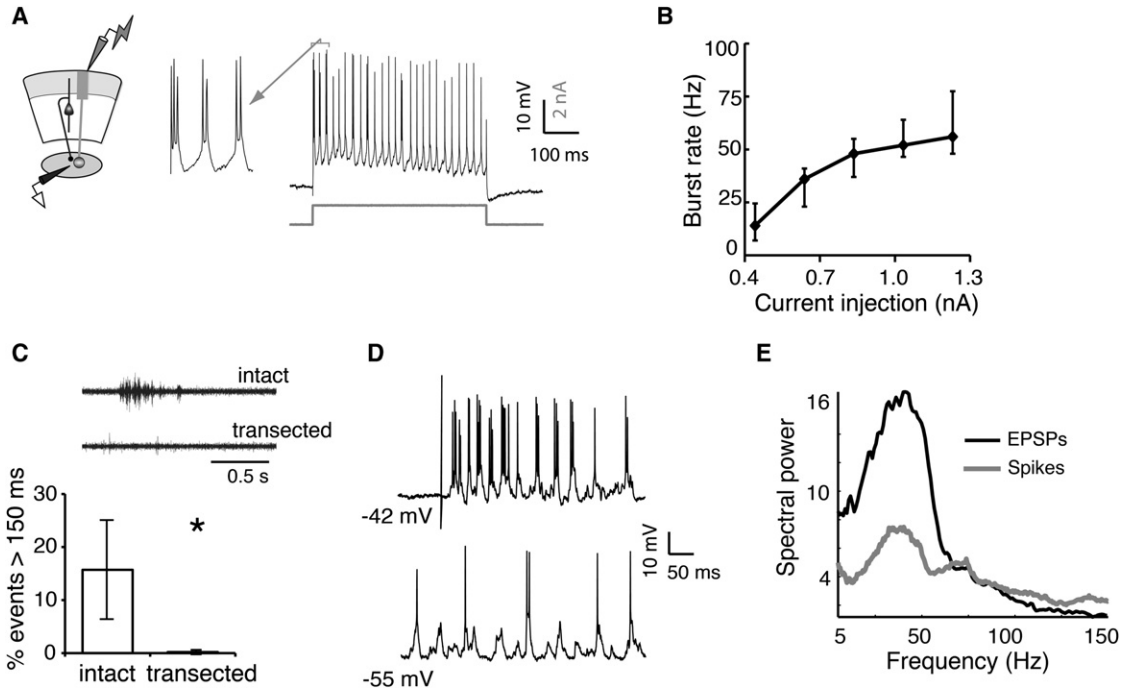

Figure 5. Ipc Neurons Burst at Gamma Frequencies but Require Persistent Input

(A) Left, schematic illustrating recording configuration in the Ipc. Right, intracellular recording from an Ipc neuron. A step depolarization (indicated by gray line below trace) induced a regular pattern of bursting.

(B) Step depolarizations of various amplitudes increased burst rate between 14 and 56 Hz (n = 5). Points on line represent median values, lower and upper whiskers represent 25th and 75th percentiles.

(C) Top, example of a spontaneous, persistent oscillation recorded in the Ipc in intact slices, but not in transected slices. Bottom, spontaneous, persistent oscillations recorded in the Ipc are eliminated in transected slices. In intact slices (n = 6), 15 ± 9% of spontaneous oscillations persist for greater than 150 ms, while in transected slices (n = 5), only 0.2 ± 0.4% of spontaneous events with gamma power persisted longer than 150 ms ($p < 0.005$, U-test). See Figure S4 for more details.

(D) In an intact slice, intracellular recordings in the Ipc reveal periodicity. Top, periodic bursting of an Ipc neuron following retinal afferent stimulation. Bottom, periodic EPSPs were revealed in the neuron upon hyperpolarization of the membrane potential.

(E) Average power spectrum of postsynaptic potentials (black, n = 5) indicates strong gamma periodicity in the synaptic input to Ipc neurons. Spectrum of the spiking responses (gray) shows that Ipc spike periodicity matched the frequency of the synaptic input.

the structure of the oscillations in the intact slice (Figure 3) should alter them in the same way when applied specifically to the OT. First, we tested the effects of the NMDA-R blocker APV on induced gamma oscillations in the isolated OT. In transected slices, bath application of APV substantially reduced the duration (11.1% of control, $p < 0.001$, n = 8; Figures 7, S6A, S6B, and S6C) and power (49.3% of control, $p < 0.001$, Friedman test, n = 8) of activity in the i/dOT. Moreover, increasing the strength of afferent stimulation by 3–4× in the presence of APV did not increase the duration of the oscillations (Figure S6D), suggesting that the effect of APV was not merely to reduce the general excitability of the OT circuitry. In sum, these data suggested that NMDA-R mediated glutamatergic transmission in the i/dOT was essential for the persistence of the oscillations.

Next, we tested the effects of focal application of the GABA-R blocker PTX to the OT in intact slices. Recall that PTX, when bath-applied to intact slices, eliminated gamma periodicity (Figure 3A). We puffed PTX focally onto either the OT or the Ipc with a micropipette while recording activity in the sOT in intact midbrain slices. Both the OT and the Ipc are innervated by GABAergic circuits, as indicated by the presence of parvalbumin immunoreactivity in both structures (Figure 8A). When applied to the OT, puffs of PTX transiently changed gamma oscillations into episodes of high-frequency spiking, mimicking the results of bath application (Figures 8B, 8C, and S7A; duration: 33% of control, $p > 0.5$; power: 31% of control, $p < 0.001$, Friedman test, n = 7). In contrast, puffs of PTX applied to the Ipc in the same slice did not alter the periodic structure of gamma oscillations in the sOT (Figures 8D, 8E, and S7B; duration: 88% of control, $p > 0.3$; power: 74% of control, $p > 0.5$, n = 7). These results demonstrate conclusively that inhibition in the OT regulates the gamma periodicity of the midbrain oscillator.

DISCUSSION

This study demonstrates that gamma oscillations can be induced in an in vitro slice preparation of the avian midbrain network and that these oscillations strongly resemble those induced by salient sensory stimuli in vivo. The synaptic mechanisms that regulate the frequency, power, and duration of the

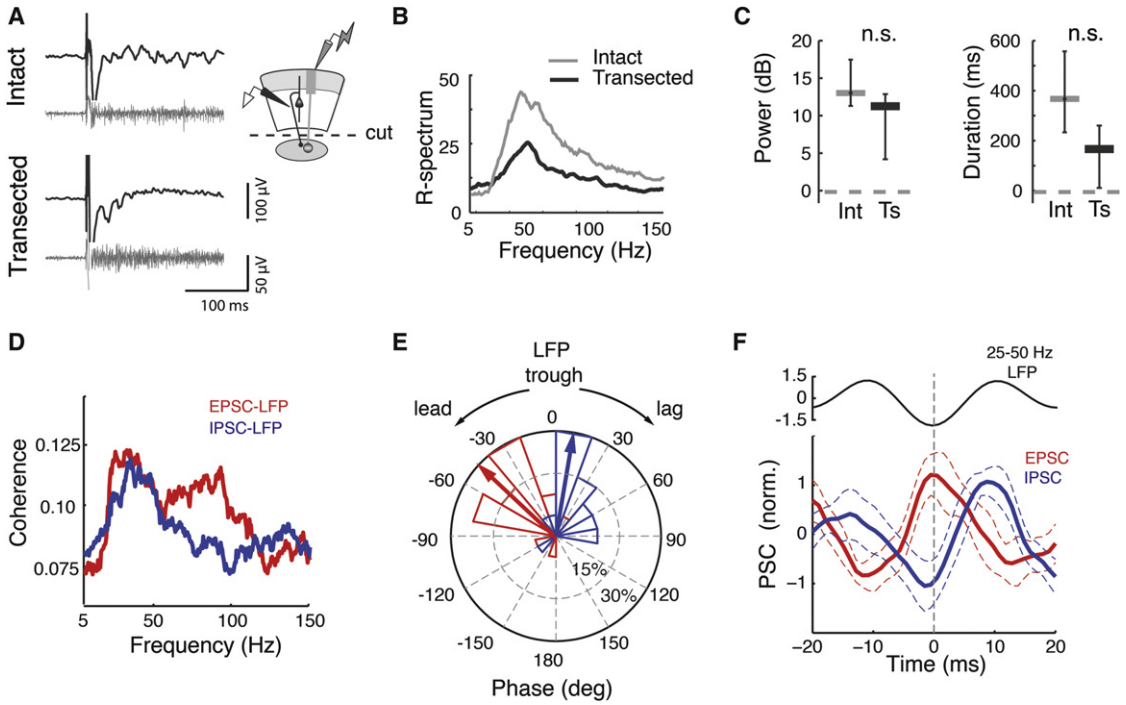

Figure 6. The i/dOT Generates Persistent Gamma Oscillations without Ipc Connectivity.

Conventions as in Figure 3.

(A) Left, evoked, persistent gamma oscillations recorded in the i/dOT are observed both in an intact slice (top) and in a transected slice (bottom). These recordings were made simultaneously with recordings in the sOT described in Figure 4. Right, schematic illustrating recording configuration in the i/dOT, and transection of connections with the Ipc.

(B) Average R-spectra for responses in the i/dOT in intact (gray) and transected (black) slices (n = 10 in each condition) show similar profiles.

(C) Left, gamma power (25–50 Hz, in dB) of oscillations in i/dOT was not significantly different in intact (gray) and transected (black) slices. Intact = 13.2 dB, transected = 11.4 dB, $p > 0.2$, U-test, n = 10. Right, durations of gamma oscillations in the i/dOT were not significantly different in intact (gray) and transected (black) slices. Median durations for intact slices = 373 ms, transected = 172 ms, $p > 0.1$.

(D) Coherence between the extracellular LFP and the onset of simultaneously recorded EPSCs recorded at −65 mV (red), or IPSCs recorded at 0 mV (blue), indicates peak power in the lower gamma-band (n = 17 LFP-neuron pairs).

(E) Phase of EPSCs (red) leads IPSCs (blue) relative to the trough of the 25–50 Hz LFP oscillations. Negative angles represent onsets preceding (leading) the trough, and positive angles represent onsets following (lagging) the trough. Radial axis: percent of sites, outer circle represents 30% of sites. Wedges: histogram of the phase distribution. Arrows: Mean of the phase distribution (n = 17).

(F) LFP-trough triggered averages of the EPSC (red) and IPSC (blue). For comparison with IPSC peak times, EPSCs have been inverted relative to standard convention, such that the peak of the EPSC represents the maximal inward current. Dashed vertical line: t = 0 at LFP trough. Dashed lines: 95% confidence intervals of the mean waveform across n = 17 sites. Top inset: mean 25–50 Hz LFP oscillation cycle. All data averaged over 7,000 LFP cycles.

oscillations are similar to those that regulate gamma oscillations in mammalian forebrain structures. The source of the midbrain oscillations is the i/dOT. Rhythmic output from the i/dOT entrains periodic burst firing in the cholinergic nucleus Ipc, and the Ipc broadcasts the oscillations to the sOT. In the discussion that follows, we compare the mechanisms that regulate midbrain gamma oscillations with those that regulate gamma oscillations in the mammalian forebrain. We also consider the potential importance of the oscillations to information processing in this attention-related network.

Gamma Oscillations across Brain Regions and Phylogeny

Gamma oscillations have been observed in many mammalian brain structures, including the neocortex (Buhl et al., 1998), hippocampus (Traub et al., 1996), olfactory bulb, (Bressler and Freeman, 1980), cerebellum (Middleton et al., 2008), and SC (Brecht et al., 1999). The pharmacology of the gamma oscillations in the avian midbrain is strikingly similar to those observed in the mammalian neocortex and hippocampus: GABA-Rs regulate the periodicity of the oscillations, ACh-Rs modulate the excitability of the oscillator, and NMDA-Rs are essential for the persistence of the oscillations. Moreover, the microstructure of the oscillations in the avian sOT includes bursts of spikes that are tightly phase-locked to gamma LFP oscillations, similar to the phase-locked bursts of chattering cells during gamma LFP oscillations in the mammalian neocortex (Gray and McCormick, 1996).

In addition, neural activity with gamma periodicity has been observed in a wide range of vertebrate species, including species of birds (Marín et al., 2005; Neuenschwander et al., 1996), amphibians (Arai et al., 2004; Ishikane et al., 2005), and fish (Ramcharitar et al., 2006). The gamma oscillations that we recorded in OT slices from young chickens are remarkably

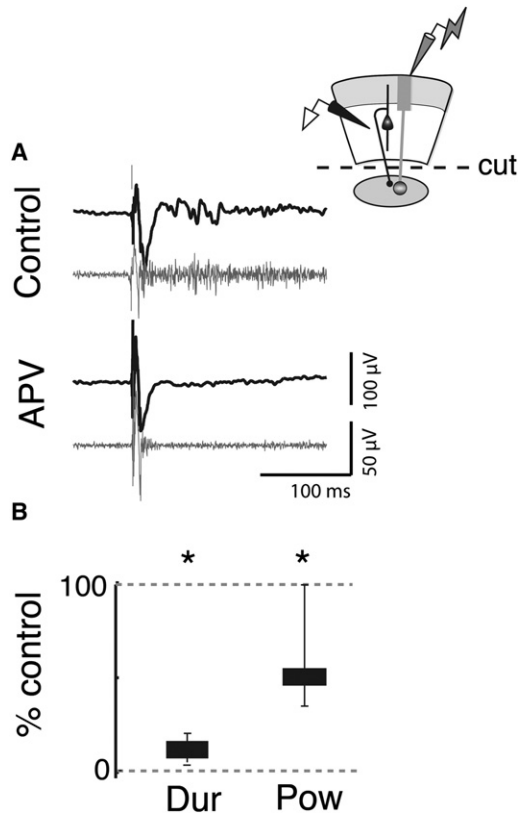

Figure 7. NMDA-Rs Regulate the Persistence of Oscillations in the i/dOT

Conventions are as in Figure 3.

(A) Left, persistent gamma oscillations recorded in the i/dOT in transected slices (top) are substantially shortened following application of 50 μM APV to the bath (bottom). Scale bar is 100 ms. Upper right, schematic illustrating recording configuration in the i/dOT in transected slices.

(B) Gamma durations are significantly reduced following APV application. APV condition = 11.1% of control ($p < 0.001$, Friedman test, $n = 8$). Although reduced, some gamma power remained in the i/dOT during an early period in the response. To make accurate spectral estimates, power was measured over a 50 ms window (Experimental Procedures); power = 49.3% of control ($p < 0.001$, $n = 8$).

similar to those we recorded in vivo from adult owls, despite substantial differences between the species: chickens have panoramic vision, are diurnal, and are prey, whereas owls have stereoscopic vision, are nocturnal, and are predators. Thus, the findings reported here provide more evidence that circuitry for generating gamma oscillations and mechanisms that regulate oscillation structure are conserved across embryologically distinct regions of the brain as well as across phylogeny.

The Role of Excitation and Inhibition in Generating Persistent Gamma Oscillations

A recurrent circuit of excitatory and inhibitory neurons is common to many brain structures that generate gamma oscillations (Bartos et al., 2007). In these circuits, slow excitatory synapses provide sustained depolarizing drive, whereas synchronous firing among inhibitory interneurons provides rhythmic inhibition with gamma periodicity. Cholinergic input can modulate both excitatory and inhibitory neurons but tends to increase overall excitability of a network (Hasselmo and McGaughy, 2004). Consistent with these studies, we demonstrate that, in the avian midbrain network, NMDA-Rs enable the persistence of gamma oscillations, ionotropic GABA-Rs regulate their periodicity, and ACh-Rs regulate overall excitability.

The Role of NMDA-Rs in Gamma-Generating Circuits

The contribution of NMDA-Rs to gamma oscillations in the mammalian neocortex and hippocampus is controversial. The effects of blocking NMDA-Rs differ greatly depending on whether experiments were done in vivo or in vitro and on how the oscillations were induced. When studied in vivo, blocking NMDA-Rs typically results in an increase in cortical gamma power, possibly due to a differential effect of blocking NMDA-Rs on a subset of inhibitory neurons (Carlén et al., 2011; Korotkova et al., 2010). In contrast, most studies performed in vitro report no effect of blocking NMDA-RS when oscillations are induced by adding cholinergic or glutamatergic agonists to the bath (Roopun et al., 2008). In the latter experiments, the added agonists may have provided the sustained depolarization necessary to maintain oscillations by acting through NMDAR-independent mechanisms, rendering NMDA-R blockade ineffective.

Here, we show that persistent activity in the avian OT depends on a circuit that utilizes NMDA-Rs. The circuit also generates gamma periodicity. However, the rhythmicity and the persistence represent two separable components of the circuit. In our experiments, pharmacological agents were not required to produce oscillations. Hence, our results are consistent with studies that show a marked reduction in the duration of gamma oscillations resulting from NMDA-R blockade when such oscillations are induced in slices without pharmacological agents (Gandal et al., 2011).

Long-lasting currents with kinetics similar to NMDA-R currents have been suggested to generate and maintain persistent activity in a variety of brain structures, both in vivo and in vitro (McCormick et al., 2003; Seung et al., 2000; Wang, 1999) including in the OT/SC (Isa and Hall, 2009). However, no gamma oscillations were observed in previous in vitro studies that showed persistent activity in the OT/SC. Key differences from our study are that connectivity with cholinergic isthmic circuitry was probably not maintained and GABA-R antagonists were added to the bath to enhance network excitability (Isa and Hall, 2009; Pratt et al., 2008).

The Role of GABA-Rs in Gamma-Generating Circuits

As in the forebrain (Bartos et al., 2007), ionotropic GABA-R currents regulate the periodicity of gamma oscillations in the avian midbrain. Antagonizing GABA-Rs with PTX transformed gamma periodicity into bouts of persistent, high-frequency firing. Alternatively, enhancing GABA-R function with pentobarbital slowed the frequency of the oscillations. We also observed rhythmic IPSCs in the i/dOT that exhibited phase coherence with the LFP in the gamma band. In many mammalian forebrain structures, parvalbumin-positive interneurons are specifically implicated in the generation of gamma (Cardin et al., 2009; Sohal et al., 2009). While the present study does not implicate a specific class of interneurons in gamma generation, immunostaining reveals a population of parvalbumin positive neurons that are clustered in layer 10a of the i/dOT (Figure 8A).

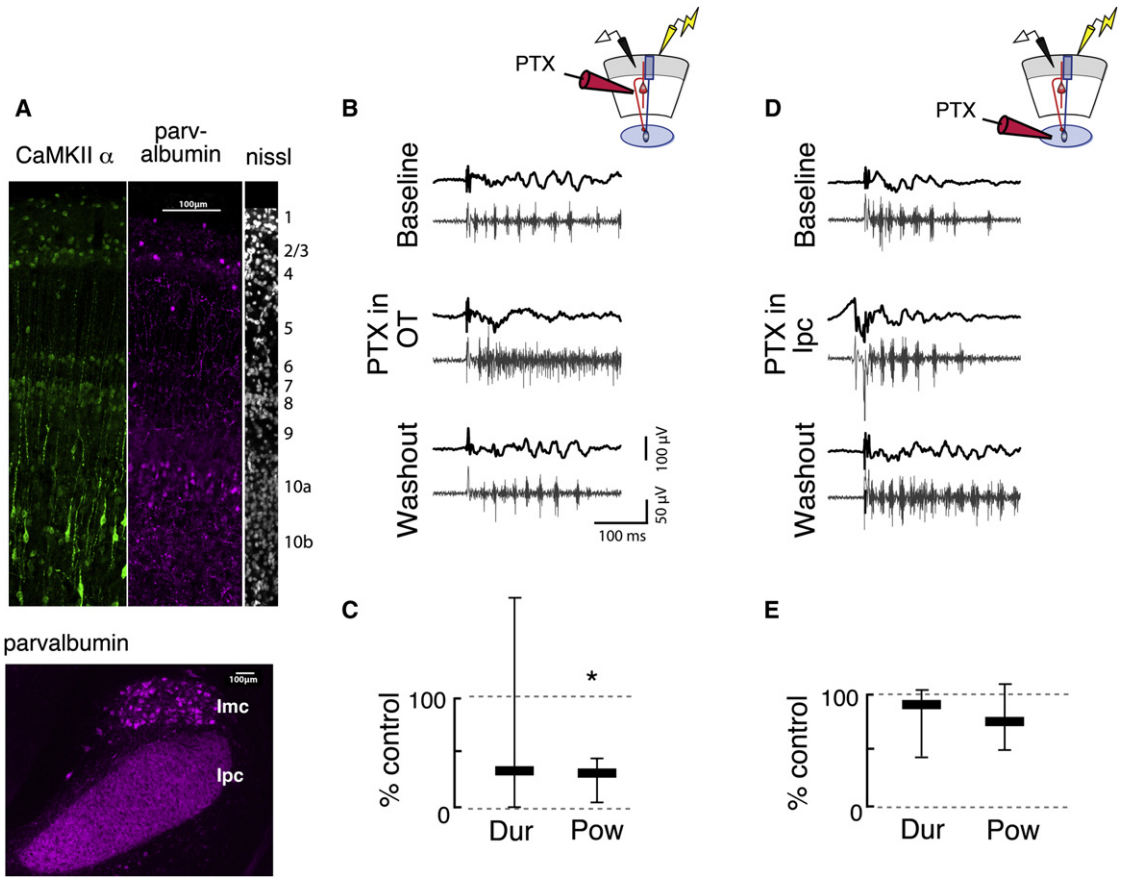

Figure 8. Focal Application of Picrotoxin to the OT, but Not to the Ipc, Alters Oscillation Structure

Conventions are as in Figure 3.

(A) Parvalbumin and CaMKII proteins show enhanced immunoreactivity in layer 10 of the i/dOT. Left (green), CaMKII, a marker for putative excitatory neurons, in the top 10 layers of the OT. Middle (purple), parvalbumin, a marker for putative inhibitory neurons, in the top 10 layers of the OT. Right (white), Nissl stain, showing the layers of the OT. Bottom, inhibitory innervation of the Ipc. Parvalbumin is expressed highly in the neuropil in the Ipc, but not in somata. Parvalbumin is expressed somatically in the GABAergic nucleus isthmi pars magnocellularis (Imc).

(B) Left, gamma oscillations recorded in the sOT of intact slices (top) are transiently converted to high-frequency events with no appreciable gamma power following a puff of PTX (0.1–1 mM) to the OT (middle). Gamma oscillations return shortly after the puff (bottom). Upper right, schematic illustrating recording configuration in sOT while puffing PTX in the OT.

(C) Duration and power of gamma oscillations is significantly reduced following PTX puff in the OT (duration: 33% of control, power: 31% of control, $p < 0.001$, Friedman test, $n = 7$).

(D) Left, gamma oscillations recorded in the sOT (top) are not affected by a puff of PTX to the Ipc (middle). Upper right, schematic illustrating recording configuration in sOT while puffing PTX in the Ipc.

(E) Duration and power of gamma oscillations were unaffected in the evoked response following PTX puff into the Ipc (duration: 88% of control, $p > 0.3$; power: 74% of control, $p > 0.5$, Friedman test, $n = 7$).

The Role of ACh-Rs in Regulating the Excitability of Gamma-Generating Circuits

ACh-Rs regulate the overall excitability of the midbrain oscillator. Blockade of AChRs reduces the duration and power of the oscillations without affecting their periodicity. These effects of ACh could be mediated by increasing the efficacy of retinal afferents presynaptically. Previous evidence indicates that ACh facilitates glutamatergic transmission in the cortex (Gil et al., 1997; Hasselmo and McGaughy, 2004) and in the OT (King, 1990). ACh also modulates the excitability of both excitatory and inhibitory neurons in the forebrain (Hasselmo and McGaughy, 2004) and the OT/SC (Endo et al., 2005; Lee et al., 2001). A combination of these pre- and postsynaptic effects likely explains the decrease in oscillation power and duration that we observed after ACh-R blockade (Figure 3D). However, more investigation is required to understand how ACh modulates the various elements utilized by the midbrain oscillator.

The isthmic nuclei, including the Ipc and SLu, constitute an important source of ACh in the OT (Wang et al., 2006). Cholinergic inputs from the isthmic nuclei, which remained intact in our preparation, have been shown in other preparations to regulate the excitability of OT circuitry (Dudkin and Gruberg, 2003; King and Schmidt, 1991). We found that transection of Ipc inputs to the OT eliminated gamma oscillations in the sOT entirely

(Figure 4). Compared with this dramatic effect, the reduction in gamma power following AChR blockade was modest (Figure 3D), suggesting that the contribution of Ipc input to the oscillations is not mediated entirely by AChR activation. Possible alternate explanations include corelease of glutamate from Ipc axons (Islam and Atoji, 2008) and electrogenic effects of synchronized Ipc action potentials as they invade the highly organized and ramified Ipc axons in the superficial layers (Figure S3A). Alternatively, the effects of blocking AChRs on the power and duration of gamma oscillations could have resulted, at least in part, from the blockade of transmission by cholinergic interneurons that are resident to the OT (Sorenson et al., 1989). Further experiments are necessary to determine the sources of ACh in the midbrain that contribute to the excitability of the midbrain oscillator.

Candidate Tectal Circuitry Underlying the Oscillations

The data reported here indicate that a gamma-generating circuit exists in the i/dOT. We observed persistent gamma rhythmicity both in the LFP and at the level of excitatory and inhibitory synaptic currents in individual neurons in layer 10. A population of putatively inhibitory parvalbumin-positive neurons cluster in layer 10a of the i/dOT (Figure 8A). Putatively excitatory, CaMKIIα-positive neurons are located in layer 10b (Figure 8A), and neurons in layer 10b project to the isthmic nuclei and other downstream targets. The interactions of these inhibitory and excitatory neurons might constitute the midbrain gamma generator. Future research will test the validity of this hypothesis.

We did not find evidence of a persistent oscillator in the sOT. Following Ipc transection, retinal afferent stimulation continued to evoke oscillatory activity in the i/dOT but not in the sOT. Moreover, LFP oscillations in the sOT depended on Ipc input, which was periodic, and they reflected cycle-by-cycle variations in Ipc input, consistent with previous reports of a tight relationship between spike activity in the Ipc and the sOT (Marín et al., 2005).

Our results do not rule out the possibility, however, of additional oscillatory circuitry in the sOT that might be revealed by pharmacological manipulations or be modulated by direct i/dOT to sOT connections. An inhibitory feedback pathway from the i/dOT to sOT has been described in the SC and OT (Hunt and Künzle, 1976; Phongphanphanee et al., 2011). This pathway, posited to mediate saccadic suppression, might suppress oscillations during saccadic eye movement. In addition, physiological evidence suggests an excitatory projection from the i/dOT to the sOT (Vokoun et al., 2010; Goldberg and Wurtz, 1972), although such a pathway from the i/dOT to the sOT has not been described anatomically. Further research is required to determine whether such projections participate in the oscillations. Moreover, we have only studied the effects of connections that are maintained in the slice, and the forebrain is likely to modulate the excitability and rhythmicity of the SC/OT circuitry.

Functions of the Midbrain Oscillator

We have shown that the OT, a midbrain structure that contributes to controlling the direction of gaze and the locus of attention, contains a circuit that generates brief periods of gamma oscillations. This circuit is positioned to receive ascending and descending multisensory inputs, as well as movement and attention-related signals from the forebrain (Knudsen, 2011). We hypothesize that these inputs to the i/dOT act via NMDA-R-rich synapses to generate space-specific, persistent activity and that this activity is temporally sculpted into gamma oscillations by local inhibitory circuitry.

Once activated, the broadband oscillator in the i/dOT entrains Ipc neurons to burst with low gamma periodicity, and Ipc neurons broadcast this signal to the sOT via densely ramifying axonal projections (Figure S3A). This organization could provide a channel of synchronized activity across the OT layers. Thus, the rhythmic bursting of Ipc neurons could affect both input and output efficacies in the OT. First, such rhythmic bursting causes synchronized phasic release of ACh in a highly localized spatial column, potentially enhancing the sensitivity of the OT to visual inputs from a specific region of space within a gamma cycle. Second, the bursts create large amplitude LFP oscillations in the sOT that could synchronize the firing of OT neurons by ephaptic coupling (Anastassiou et al., 2011; Fröhlich and McCormick, 2010). Consistent with both of these mechanisms for temporal coding is the observation of spike-field coherence in the gamma-band in the avian i/dOT in vivo (Sridharan et al., 2011). This gamma-synchronized signal occurs within a spatially restricted portion of the tectal space map, in that gamma oscillations exhibit spatial tuning to sensory stimuli that is comparable to the tuning of single neurons.

Synchronization of OT output spikes could cause them to be more effective in driving postsynaptic targets (Fries, 2009). In addition, the rhythmic, synchronized discharges could create a channel for the midbrain network to route signals to particular downstream descending (brainstem) or ascending (thalamic and forebrain) circuits, similar to the channels proposed for cortico-cortical communication (Akam and Kullmann, 2010; Gregoriou et al., 2009). Consistent with this hypothesis, stimulus-driven, coherent oscillations have been reported between the OT and one of its thalamic targets (Marín et al., 2007). Furthermore, synchronous microstimulation of two points in the SC space map yields quantitatively different neural computations and motor outputs than does asynchronous stimulation (Brecht et al., 2004). Thus, synchrony appears to be utilized and transmitted by local OT/SC circuits.

The persistence of the oscillations could act as a short-term memory of the locations of salient stimuli, enabling crossmodal and top-down enhancement of sensory responses across brief periods of time ($\sim$100 ms). For example, a salient, spatially localized *auditory* stimulus that activates the gamma oscillator in the multisensory i/dOT would, via the Ipc circuit, increase the sensitivity of sOT neurons to subsequent *visual* stimuli from the same location in space. Thus, persistence may be essential for integrating sensory information from different modalities and from different parts of the brain that reaches the OT with different delays.

The induction of gamma oscillations by sensory stimuli and the modulation of gamma power by attention are prominent phenomena in the mammalian forebrain (Fries, 2009). The discovery that the OT contains its own persistent gamma generator is important in the context of recent studies that implicate the OT as a critical node in the network of brain structures that mediate gaze control and spatial attention (Knudsen, 2011; Lovejoy and Krauzlis, 2009). The spatial separation and

accessibility of the various inputs, outputs, and component cell-types that make up this attention-related midbrain network provide a unique opportunity for understanding the circuit mechanisms of gamma oscillations and their influence on information processing at an unprecedented level of detail.

EXPERIMENTAL PROCEDURES

More details on these methods, as well as additional methods and analyses, can be found in Supplemental Information.

In Vivo Recordings

All animals were treated in accordance with institutional guidelines. Acquisition and analysis of field recordings in vivo from the barn owl optic tectum (shown in Figures 1, S1, and S5) followed procedures described in (Sridharan et al., 2011).

In Vitro Slice Preparation

All animals were treated in accordance with institutional guidelines. White Leghorn chicks (Gallus gallus), aged p1–p6, were anesthetized with isoflurane, decapitated, and the brains were removed and immersed in a cutting solution (4°C) containing 234 mM sucrose, 11 mM glucose, 24 mM $NaHCO_3$, 2.5 mM KCl, 1.25 mM NaH_2PO_4, 10 mM $MgSO_4$, and 0.5 mM $CaCl_2$, aerated with 95% O_2 and 5% CO_2. Tecta were dissected and embedded in low melting temperature agarose (Sigma, A2756). Transverse slices (400 μm) were cut with a vibrating slicer (Leica VT1200). Slices were incubated in oxygenated artificial cerebrospinal fluid (ACSF) containing 126 mM NaCl, 26 mM $NaHCO_3$, 1.25 mM NaH_2PO_4, 2 mM $CaCl_2$, and 10 mM glucose; $MgSO_4$ and KCl were varied such that Mg^{2+}: K^+ was 2: 2.5 mM or 1:3.5 mM; (pH 7.4) Slices were bathed at 34°C for 20–30 min and, subsequently, at room temperature for a minimum of 30 min before being transferred to the recording chamber.

In Vitro Slice Recordings

Extracellular recordings were obtained at 34°C in a humidified oxygenated interface chamber, using tungsten electrodes (50–100 kΩ), amplified 50,000×, digitized by a Digidata (1200 series, Molec Devices Corp) at 10 kHz, and acquired using pClamp software. Signals were bandpass-filtered from 5 Hz–5 kHz.

Sharp electrode intracellular recordings were performed in the interface chamber with glass pipettes pulled and beveled to a final resistance of 80–90 MΩ and filled with 1 M K-acetate internal solution. Bridge balance was manually adjusted throughout the recordings. Whole-cell (WCp) and cell-attached (CAp) patch recordings were performed in a submerged chamber, with ACSF heated to 32–34°C. For CAp recordings, 8–11 MΩ pipettes were filled with ACSF. For WCp recordings, 4–7 MΩ pipettes were filled with Cs-gluconate (130 mM), CsCl (10 mM), NaCl (2 mM), HEPES (10 mM), or EGTA (4 mM). Cells with series resistance < 35 MΩ and that did not have resistance fluctuate by more than 25% were used for analysis. Series resistance was not compensated but Vm was corrected for a −16 mV junction potential.

Retinal afferents were stimulated with constant current of 10–50 μA, lasting 50–100 μs, using theta-glass electrodes pulled as patch pipettes and filled with ACSF.

Drugs were prepared from stocks to the following final dilutions: Atropine sulfate (Sigma, A 0257), 5 μM; dihydro-β-erythrodine (DHβE) (Tocris Bioscience, 2349), 40 μM; DL-APV (Sigma, A5282), 50 μM; Pentobarbital (Sigma, P3761), 5-10 μM; Picrotoxin (Sigma, P1675), 10 μM (dissolved in DMSO).

LFP Preprocessing

LFP processing was performed using Matlab (2007a, The MathWorks, Natick, MA, USA) to remove line noise, and downsampled to 1kHz (see Supplemental Information).

Computing the Duration and Power in the OT

For every trial, the evoked response was examined from 50–2,500 ms after the electrical stimulus. The first 50 ms of the response was excluded to avoid contamination by the stimulation artifact. The signal was band-pass filtered in the low gamma range (25–50 Hz). A baseline was computed from the root-mean-squared (rms) values in nonoverlapping 50 ms bins, 350 ms prior to the stimulus. For each trial, we computed the rms value of the response in overlapping, sliding windows of 50 ms duration each, sliding in 1 ms steps. The duration δ was defined as the point when rms values in more than 40 out of 50 (80%) successive windows fell below the 99th percentile of the null distribution (see Figure S1G for examples).

The gamma power (in dB) was obtained as follows: $p = 20*\log_{10}(R_s/R_b)$, where R_s = rms value from $t_0 + 50$ ms to $t_0 + \delta$ ms, and R_b is the rms of the baseline (time of stimulation: t_0), both computed from the gamma-band filtered signal. For plots of bath-applied drug treatment, gamma power was normalized to the control condition at that site. For estimating duration and power of the high-frequency response (Figures S2B and S2E), the same analysis was applied to 3 kHz downsampled traces and high-pass filtered at 500Hz. Computation of spontaneous event duration in lpc is described in Supplemental Information.

LFP Spectral Analysis

Spectral analysis was performed using multitaper spectral estimation with the Chronux toolbox (Mitra and Bokil, 2008). The stimulus-locked part of the response was removed by subtracting the average response across trials from each evoked response, yielding the induced power spectrum. Spectra were computed from $t_0 + 50$ ms to $t_0 + \delta$ ms, where δ = median duration of the oscillatory episode at each site for each condition. Ratio spectra (R-spectra) were computed by normalizing induced spectral power at each frequency by power at that frequency during a prestimulation baseline (t_0-δ to t_0-25 ms).

Computing Oscillation Frequencies

Peak frequencies correspond to the maximum relative power in the trial-averaged R-spectrum in the frequency range of 10–100 Hz. To estimate the gamma oscillation frequency in the drug application experiments, we measured the peak of the raw power spectrum because we were interested only in changes of peak frequency relative to control (Figures 3B, 3D, S2B, and S2D).

Computing Spectra of Membrane Potentials and Spikes (Figure 5)

For sharp electrode recordings in the lpc, we analyzed subthreshold potentials by low-pass filtering at 200 Hz and the multitaper approach for continuous signals. To compute the spectrum of the bursts, recordings were filtered between 0.5–3.5 kHz, and the spike-times extracted and analyzed with a multitaper spectral estimation algorithm for point processes (Chronux toolbox).

Statistical Tests

Median power, duration, and frequencies were compared across conditions with nonparametric statistics. We used the Friedman test (a nonparametric version of the repeated-measures ANOVA) when comparing metrics across conditions applied to the same slice (control, drug wash-in and wash-out). All other comparisons were performed with the Mann-Whitney U test. All p-values were Bonferroni-corrected for multiple comparisons where appropriate. Individual sites (n) represented separate slices, not multiple sites in a given slice. Median values were obtained from 10–40 stimulus repetitions, except for transient drug applications, for which parameters were estimated based on 2–3 repetitions.

SUPPLEMENTAL INFORMATION

Supplemental Information includes Supplemental Experimental Procedure and seven figures and can be found with this article online at doi:10.1016/j.neuron.2011.11.028.

ACKNOWLEDGMENTS

This work was supported by Stanford Dean's Postdoctoral Fellowship (C.A.G.), NEI F32 EY018787-01 (C.A.G.), NINDS NS34774 (J.R.H.), and NEI EY019179-31 (E.I.K.). Special thanks to Stefan Heller, Tom Clandinin,

Kwabena Boahen, Shreesh Mysore, Astra Bryant, and members of the Knudsen and Huguenard labs for assistance and useful discussions.

Accepted: November 23, 2011
Published: February 8, 2012

REFERENCES

Akam, T., and Kullmann, D.M. (2010). Oscillations and filtering networks support flexible routing of information. Neuron *67*, 308–320.

Anastassiou, C.A., Perin, R., Markram, H., and Koch, C. (2011). Ephaptic coupling of cortical neurons. Nat Neurosci. *14*, 217–223.

Arai, I., Yamada, Y., Asaka, T., and Tachibana, M. (2004). Light-evoked oscillatory discharges in retinal ganglion cells are generated by rhythmic synaptic inputs. J. Neurophysiol. *92*, 715–725.

Asadollahi, A., Mysore, S.P., and Knudsen, E.I. (2010). Stimulus-driven competition in a cholinergic midbrain nucleus. Nat. Neurosci. *13*, 889–895.

Bartos, M., Vida, I., and Jonas, P. (2007). Synaptic mechanisms of synchronized gamma oscillations in inhibitory interneuron networks. Nat. Rev. Neurosci. *8*, 45–56.

Brecht, M., Singer, W., and Engel, A.K. (1999). Patterns of synchronization in the superior colliculus of anesthetized cats. J. Neurosci. *19*, 3567–3579.

Brecht, M., Singer, W., and Engel, A.K. (2004). Amplitude and direction of saccadic eye movements depend on the synchronicity of collicular population activity. J. Neurophysiol. *92*, 424–432.

Bressler, S.L., and Freeman, W.J. (1980). Frequency analysis of olfactory system EEG in cat, rabbit, and rat. Electroencephalogr. Clin. Neurophysiol. *50*, 19–24.

Buhl, E.H., Tamás, G., and Fisahn, A. (1998). Cholinergic activation and tonic excitation induce persistent gamma oscillations in mouse somatosensory cortex in vitro. J. Physiol. *513*, 117–126.

Cardin, J.A., Carlén, M., Meletis, K., Knoblich, U., Zhang, F., Deisseroth, K., Tsai, L.-H., and Moore, C.I. (2009). Driving fast-spiking cells induces gamma rhythm and controls sensory responses. Nature *459*, 663–667.

Carlén, M., Meletis, K., Siegle, J.H., Cardin, J.A., Futai, K., Vierling-Claassen, D., Rühlmann, C., Jones, S.R., Deisseroth, K., Sheng, M., et al. (2011). A critical role for NMDA receptors in parvalbumin interneurons for gamma rhythm induction and behavior. Mol. Psychiatry, in press. Published online April 5, 2011. 10.1038/journal.mp.2011.31.

Dudkin, E.A., and Gruberg, E.R. (2003). Nucleus isthmi enhances calcium influx into optic nerve fiber terminals in Rana pipiens. Brain Res. *969*, 44–52.

Endo, T., Yanagawa, Y., Obata, K., and Isa, T. (2005). Nicotinic acetylcholine receptor subtypes involved in facilitation of GABAergic inhibition in mouse superficial superior colliculus. J. Neurophysiol. *94*, 3893–3902.

Engel, A.K., Fries, P., and Singer, W. (2001). Dynamic predictions: oscillations and synchrony in top-down processing. Nat. Rev. Neurosci. *2*, 704–716.

Fecteau, J.H., and Munoz, D.P. (2006). Salience, relevance, and firing: a priority map for target selection. Trends Cogn. Sci. (Regul. Ed.) *10*, 382–390.

Fisahn, A., Pike, F.G., Buhl, E.H., and Paulsen, O. (1998). Cholinergic induction of network oscillations at 40 Hz in the hippocampus in vitro. Nature *394*, 186–189.

Fries, P. (2009). Neuronal gamma-band synchronization as a fundamental process in cortical computation. Annu. Rev. Neurosci. *32*, 209–224.

Fröhlich, F., and McCormick, D.A. (2010). Endogenous electric fields may guide neocortical network activity. Neuron *67*, 129–143.

Gandal, M.J., Edgar, J.C., Klook, K., and Siegel, S.J. (2011). Gamma synchrony: Towards a translational biomarker for the treatment-resistant symptoms of schizophrenia. Neuropharmacology *62*, 1504–1518.

Gil, Z., Connors, B.W., and Amitai, Y. (1997). Differential regulation of neocortical synapses by neuromodulators and activity. Neuron *19*, 679–686.

Goldberg, M.E., and Wurtz, R.H. (1972). Activity of superior colliculus in behaving monkey. II. Effect of attention on neuronal responses. J. Neurophysiol. *35*, 560–574.

Gray, C.M., and McCormick, D.A. (1996). Chattering cells: superficial pyramidal neurons contributing to the generation of synchronous oscillations in the visual cortex. Science *274*, 109–113.

Graybiel, A.M. (1978). A satellite system of the superior colliculus: the parabigeminal nucleus and its projections to the superficial collicular layers. Brain Res. *145*, 365–374.

Gregoriou, G.G., Gotts, S.J., Zhou, H., and Desimone, R. (2009). High-frequency, long-range coupling between prefrontal and visual cortex during attention. Science *324*, 1207–1210.

Gruberg, E., Dudkin, E., Wang, Y., Marín, G., Salas, C., Sentis, E., Letelier, J., Mpodozis, J., Malpeli, J., Cui, H., et al. (2006). Influencing and interpreting visual input: the role of a visual feedback system. J. Neurosci. *26*, 10368–10371.

Hasselmo, M.E., and McGaughy, J. (2004). High acetylcholine levels set circuit dynamics for attention and encoding and low acetylcholine levels set dynamics for consolidation. Prog. Brain Res. *145*, 207–231.

Hunt, S.P., and Künzle, H. (1976). Selective uptake and transport of label within three identified neuronal systems after injection of 3H-GABA into the pigeon optic tectum: an autoradiographic and Golgi study. J. Comp. Neurol. *170*, 173–189.

Isa, T., and Hall, W. (2009). Exploring the Superior Colliculus In Vitro. J. Neurophysiol..

Ishikane, H., Gangi, M., Honda, S., and Tachibana, M. (2005). Synchronized retinal oscillations encode essential information for escape behavior in frogs. Nat. Neurosci. *8*, 1087–1095.

Islam, M.R., and Atoji, Y. (2008). Distribution of vesicular glutamate transporter 2 and glutamate receptor 1 mRNA in the central nervous system of the pigeon (Columba livia). J. Comp. Neurol. *511*, 658–677.

King, W.M. (1990). Nicotinic depolarization of optic nerve terminals augments synaptic transmission. Brain Res. *527*, 150–154.

King, W.M., and Schmidt, J.T. (1991). The long latency component of retinotectal transmission: enhancement by stimulation of nucleus isthmi or tectobulbar tract and block by nicotinic cholinergic antagonists. Neuroscience *40*, 701–712.

Knudsen, E.I. (2011). Control from below: the role of a midbrain network in spatial attention. Eur. J. Neurosci. *33*, 1961–1972.

Korotkova, T., Fuchs, E.C., Ponomarenko, A., von Engelhardt, J., and Monyer, H. (2010). NMDA receptor ablation on parvalbumin-positive interneurons impairs hippocampal synchrony, spatial representations, and working memory. Neuron *68*, 557–569.

Lee, P.H., Schmidt, M., and Hall, W.C. (2001). Excitatory and inhibitory circuitry in the superficial gray layer of the superior colliculus. J. Neurosci. *21*, 8145–8153.

Lovejoy, L.P., and Krauzlis, R.J. (2009). Inactivation of primate superior colliculus impairs covert selection of signals for perceptual judgments. Nat. Neurosci. *13*, 261–266.

Marín, G., Mpodozis, J., Sentis, E., Ossandón, T., and Letelier, J.C. (2005). Oscillatory bursts in the optic tectum of birds represent re-entrant signals from the nucleus isthmi pars parvocellularis. J. Neurosci. *25*, 7081–7089.

Marín, G., Salas, C., Sentis, E., Rojas, X., Letelier, J.C., and Mpodozis, J. (2007). A cholinergic gating mechanism controlled by competitive interactions in the optic tectum of the pigeon. J. Neurosci. *27*, 8112–8121.

McCormick, D.A., Shu, Y., Hasenstaub, A., Sanchez-Vives, M., Badoual, M., and Bal, T. (2003). Persistent cortical activity: mechanisms of generation and effects on neuronal excitability. Cereb. Cortex *13*, 1219–1231.

Middleton, S.J., Racca, C., Cunningham, M.O., Traub, R.D., Monyer, H., Knöpfel, T., Schofield, I.S., Jenkins, A., and Whittington, M.A. (2008). High-frequency network oscillations in cerebellar cortex. Neuron *58*, 763–774.

Mitra, P., and Bokil, H. (2008). Observed Brain Dynamics (New York: Oxford University Press).

Mysore, S.P., Asadollahi, A., and Knudsen, E.I. (2010). Global inhibition and stimulus competition in the owl optic tectum. J. Neurosci. *30*, 1727–1738.

Neuenschwander, S., Engel, A.K., König, P., Singer, W., and Varela, F.J. (1996). Synchronization of neuronal responses in the optic tectum of awake pigeons. Vis. Neurosci. *13*, 575–584.

Phongphanphanee, P., Mizuno, F., Lee, P.H., Yanagawa, Y., Isa, T., and Hall, W.C. (2011). A circuit model for saccadic suppression in the superior colliculus. J. Neurosci. *31*, 1949–1954.

Pratt, K.G., Dong, W., and Aizenman, C.D. (2008). Development and spike timing-dependent plasticity of recurrent excitation in the Xenopus optic tectum. Nat. Neurosci. *11*, 467–475.

Ramcharitar, J.U., Tan, E.W., and Fortune, E.S. (2006). Global electrosensory oscillations enhance directional responses of midbrain neurons in eigenmannia. J. Neurophysiol. *96*, 2319–2326.

Rodriguez, R., Kallenbach, U., Singer, W., and Munk, M.H.J. (2004). Short- and long-term effects of cholinergic modulation on gamma oscillations and response synchronization in the visual cortex. J. Neurosci. *24*, 10369–10378.

Roopun, A.K., Cunningham, M.O., Racca, C., Alter, K., Traub, R.D., and Whittington, M.A. (2008). Region-specific changes in gamma and beta2 rhythms in NMDA receptor dysfunction models of schizophrenia. Schizophr. Bull. *34*, 962–973.

Roopun, A.K., Lebeau, F.E.N., Ramell, J., Cunningham, M.O., Traub, R.D., and Whittington, M.A. (2010). Cholinergic neuromodulation controls directed temporal communication in neocortex in vitro. Front Neural Circuits *4*, 8.

Seung, H.S., Lee, D.D., Reis, B.Y., and Tank, D.W. (2000). Stability of the memory of eye position in a recurrent network of conductance-based model neurons. Neuron *26*, 259–271.

Sohal, V.S., Zhang, F., Yizhar, O., and Deisseroth, K. (2009). Parvalbumin neurons and gamma rhythms enhance cortical circuit performance. Nature *459*, 698–702.

Sorenson, E.M., Parkinson, D., Dahl, J.L., and Chiappinelli, V.A. (1989). Immunohistochemical localization of choline acetyltransferase in the chicken mesencephalon. J. Comp. Neurol. *281*, 641–657.

Sridharan, D., Boahen, K., and Knudsen, E.I. (2011). Space coding by gamma oscillations in the barn owl optic tectum. J. Neurophysiol. *105*, 2005–2017.

Traub, R.D., Whittington, M.A., Colling, S.B., Buzsáki, G., and Jefferys, J.G. (1996). Analysis of gamma rhythms in the rat hippocampus in vitro and in vivo. J. Physiol. *493*, 471–484.

Vokoun, C.R., Jackson, M.B., and Basso, M.A. (2010). Intralaminar and interlaminar activity within the rodent superior colliculus visualized with voltage imaging. J. Neurosci. *30*, 10667–10682.

Wang, X.J. (1999). Synaptic basis of cortical persistent activity: the importance of NMDA receptors to working memory. J. Neurosci. *19*, 9587–9603.

Wang, Y., Luksch, H., Brecha, N.C., and Karten, H.J. (2006). Columnar projections from the cholinergic nucleus isthmi to the optic tectum in chicks (Gallus gallus): a possible substrate for synchronizing tectal channels. J. Comp. Neurol. *494*, 7–35.